University of Bath

Alternative formats

If you require this document in an alternative format, please contact:
openaccess@bath.ac.uk

MEASUREMENT OF HEAT TRANSFER AND FLOW STRUCTURES IN A CLOSED ROTATING CAVITY

Richard W. Jackson, Hui Tang, James A. Scobie, J. Michael Owen and Gary D. Lock

r.w.jackson@bath.ac.uk, h.tang2@bath.ac.uk, j.a.scobie@bath.ac.uk, ensjmo@bath.ac.uk and g.d.lock@bath.ac.uk

Department of Mechanical Engineering, University of Bath
Bath, BA2 7AY, UK

ABSTRACT

Buoyancy-induced flow occurs inside the rotating compressor cavities of gas turbines. These cavities are usually open at the inner radius, but in some industrial gas turbines, they are effectively closed. This paper presents measurements of the disc heat transfer and rotating flow structures in a closed cavity over a wide range of engine relevant conditions. These experimentally derived distributions of disc temperature and heat flux are the first of their kind to be published. The radial distribution of the non-dimensional disc temperature virtually collapsed onto a single curve over the full experimental range. There was a small, monotonic departure from this common curve with increasing Reynolds number; this was attributed to compressibility effects where the core temperature increases as the rotational speed increases. These results imply that, if compressibility effects are negligible, all rotating closed cavities should have a disc temperature distribution uniquely related to the geometry and disc material; this is of important practical use to the engine designer. Unsteady pressure sensors detected either three or four vortex pairs across the experimental range. The number of pairs changed with Grashof number, and the structures slipped relative to the rotating discs by less than 1% of the disc speed.

1. INTRODUCTION

The operating clearance between the blade tip and the casing in the compressor of a gas turbine is governed by the radial growth of the discs, which is caused by a combination of thermal and mechanical stresses. The life of the compressor rotor is also affected by the temperatures and stresses. Compressor cavities are generally open at the inner radius, where there is a transfer of heat and momentum with an axial throughflow of cooling air. However, in some designs (principally in industrial gas turbines), the axial gap between the discs at the inner radius is very small and can even be zero (*i.e. a closed cavity*). Buoyancy-induced flow can occur in both open and closed compressor cavities.

Figure 1 shows the cross-section of the compressor of an industrial gas turbine, which contains several cavities. Labelled is an example of a closed cavity, formed between the shroud, diaphragms of the rotating discs and the cobs at low radius.

The air in the mainstream annulus is heated due to the increase in pressure, and the heat transfer to the shroud creates a radial temperature gradient within the compressor discs. Even though the cavity is closed, the radial temperature gradients can still drive buoyancy-induced flow. This results in a conjugate heat transfer system, where the temperature of the discs depends on that of the enclosed air, and vice-versa.
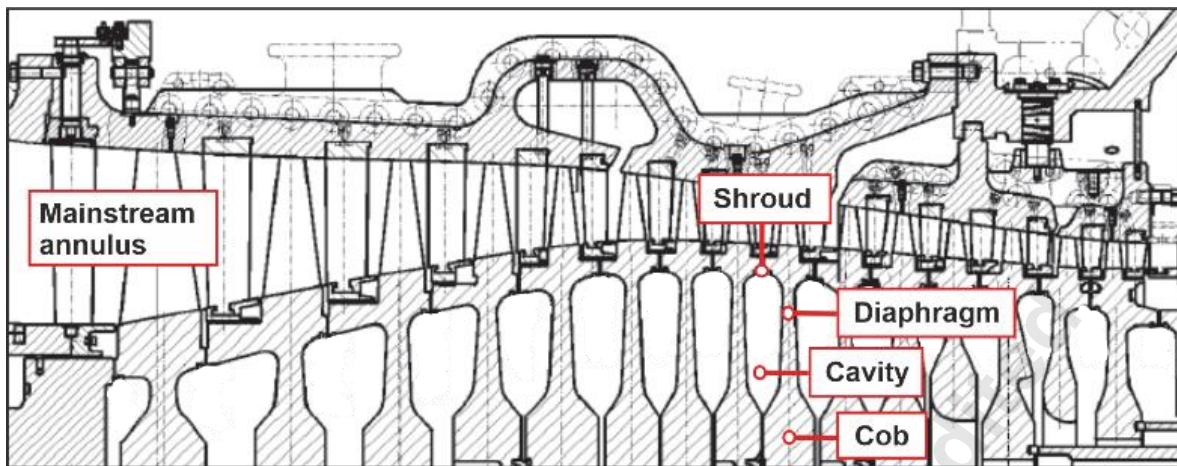
Figure 1: A cross-section through the compressor of an industrial gas turbine

(Siemens SGT6-4000F), adapted from [1].

The buoyancy-induced flow structure for an *open cavity*, was first reported in the experimental studies of Farthing *et al.* [2], and it has been observed in numerous computational and experimental research studies, *e.g.* Jackson *et al.* [3]. For a *closed cavity*, the flow structure has only been reported in computational studies, as described in Section 2.

Figure 2a shows a simplified representation of the flow structure in the inviscid rotating core of an idealized closed rotating cavity where the outer cylindrical surface (the shroud) has a higher temperature than the inner cylindrical surface (the hub). Owing to "centrifugal forces" in the rotating core, denser cold fluid tends to move radially outward; conversely, hot fluid moves radially inward. Coriolis forces are required for such radial flow to occur in the inviscid rotating core, and these forces are created by the cyclonic and anticyclonic vortices in the r-ϕ plane. The cyclonic vortices (which rotate in the same sense as the cavity) and anticyclonic vortices (which rotate in the opposite sense) produce, respectively, relative negative and positive pressures (shown by the -/+ signs in Fig. 2a),

and the circumferential pressure difference provides the Coriolis forces for the radial flow

to occur.
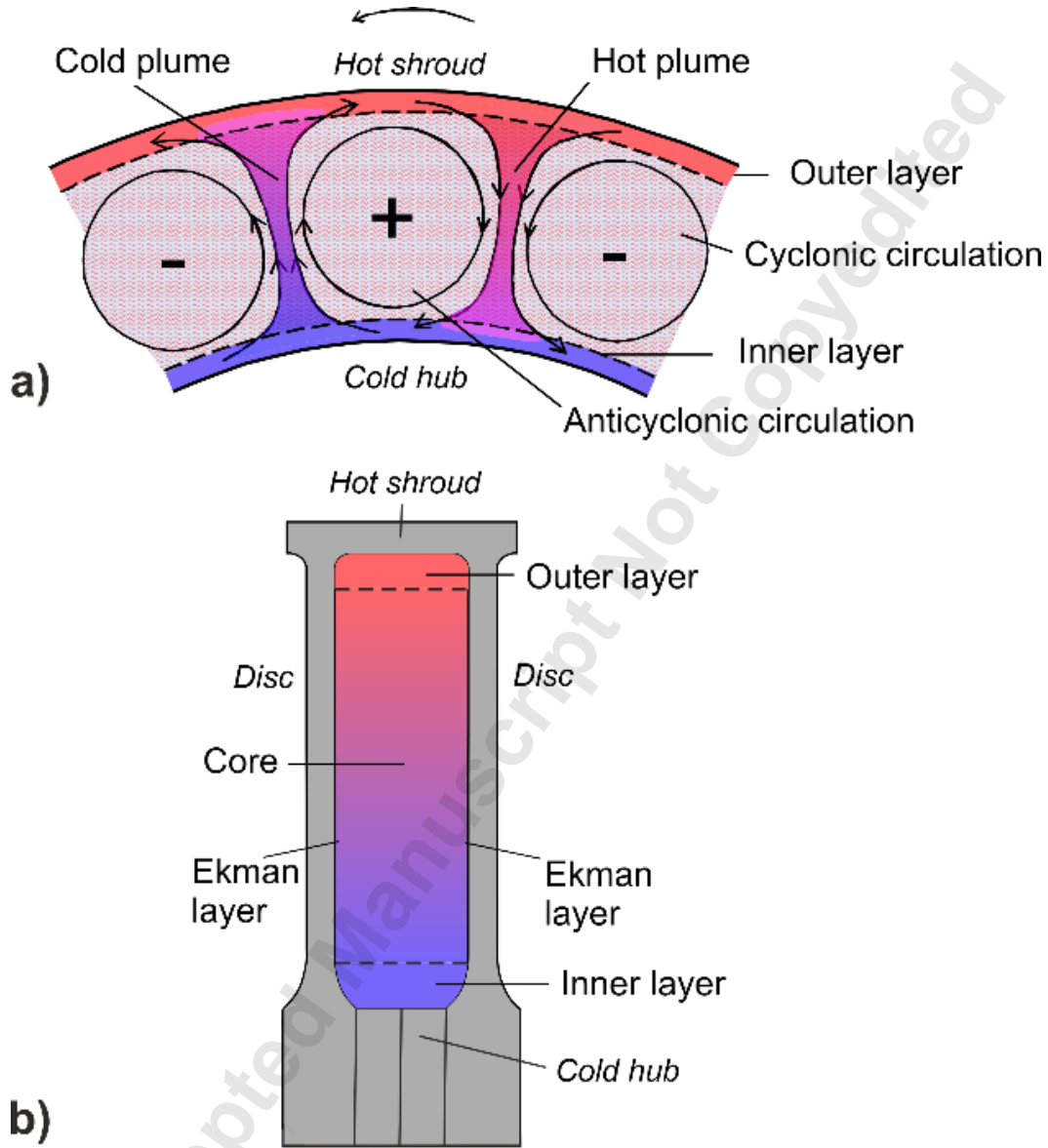
Figure 2: Simplified representation of buoyancy-induced flow inside a closed

rotating cavity, showing the *r*-ϕ plane (a) and the *r-z* plane (b).

Between one pair of vortices, a cold plume of air flows radially outward; between the

adjacent pair of vortices, a hot plume flows inward. According to the Maximum Entropy

Production principle (see [4]), the system will organize itself to form the number of vortex pairs, n, that maximize the rate of production of entropy inside the fluid, which in turn maximizes the heat transfer. An approximation for n can be obtained using the circular-vortex hypothesis:

$$\frac{a}{b} = \frac{2n - \pi}{2n + \pi} \tag{1}$$

where a and b refer to the radius of the hub and shroud (inner and outer cylinder), respectively. All symbols are defined in the nomenclature. In a closed compressor cavity, the heat transfer is principally governed by the Grashof number:

$$Gr = Re_\phi^2 \beta \Delta T \tag{2}$$

Gr is affected by the rotational Reynolds number, Re_ϕ, and the temperature difference (ΔT) between the shroud and the hub.

Figure 2b shows the simplified flow structure in the r-z plane of a closed cavity in which there is heat transfer from the discs in addition to that between the hot and cold cylindrical surfaces. In this case, thin Ekman layers can form on the discs, and circumferential shear stresses provide the Coriolis forces required for radial flow to occur inside these layers.

The total heat flow into and out of the cavity must be zero, so that the heat flow from the shroud and the net heat flow from the discs must equal the heat flow to the hub. The core of fluid between the Ekman layers must be cooler than the shroud and discs at the larger radii, and hotter at the smaller radii. Heat will therefore flow from the discs to the

air at the larger radii and from the air to the discs at the smaller radii. *There will therefore be a critical radius at which the disc heat flux is zero.*

Ekman-layer flow in a rotating cavity requires relative rotation between the discs and the core. As shown by Owen, Pincombe and Rogers [5] for isothermal source-sink flow in an open rotating cavity, radial outflow in an Ekman layer is associated with a core rotating slower than the disc; inflow is associated with a core rotating faster. In a closed cavity, relative rotation of the core creates circumferential shear stresses and hence moments on all the rotating surfaces. As the sum of the moments must be zero in a closed cavity, there will be some radial location where the direction of the core rotation changes sign. If the core rotates slower than the disc in the outer part of the cavity, it must rotate faster in the inner part; and *vice versa*.

The heat transfer behavior and flow structures within an *open* rotating cavity have previously been investigated using the Bath Compressor-Cavity Rig [3,6,7]. In this paper, the rig was reconfigured to investigate the effect of $\beta\Delta T$ and Re_ϕ (and hence, Gr) in a *closed* rotating cavity. Steady-state temperatures and unsteady pressures were measured in the central cavity of the rig. The temperatures were converted to a heat flux distribution for the discs using a Bayesian statistical method [8] that has been successfully applied for the open cavity case.

As far as the authors are aware, the heat transfer measurements presented in this paper are the first for a closed cavity since Bohn *et al.* [9]. Further, the radial distributions of disc heat flux presented here are the first experimental measurements of this kind for a closed cavity case.

Section 2 contains a brief review of the relevant literature on closed cavities. Section 3 describes the Bath Compressor-Cavity Rig and the experimental method. Section 4

summarizes the disc heat transfer results and Section 5 presents the unsteady pressure measurements. The conclusions are summarized in Section 6.

2. REVIEW OF RESEARCH ON CLOSED ROTATING CAVITIES

A comprehensive review of buoyancy-induced flow within compressor rotor cavities was provided by Owen and Long [10]. This section only reviews the research related to the flow structures and heat transfer in closed cavities.

Bohn *et al.* [9] measured the heat transfer on the cylindrical surfaces of three different closed rotating cavities (denoted A/B/C) with heated shrouds, cooled hubs and thermally insulated discs. Cavity C had radial vanes between the two discs.

The heat flux across the cylindrical surfaces was inferred from a measured temperature difference across a thermal resistance with a known thermal conductivity. Correlations were provided between the Nusselt numbers, Nu, on the cylindrical surfaces and the Rayleigh number, Ra – details of these definitions are provided in their paper. The shroud temperature, rotational speed and cavity pressure were varied over a range of $10^7 < \text{Ra} < 10^{12}$.

The correlations for the three cavities were:

$$\text{Nu}_A = 0.246 \, \text{Ra}^{0.228} \tag{3a}$$

$$\text{Nu}_B = 0.317 \, \text{Ra}^{0.211} \tag{3b}$$

$$\text{Nu}_C = 0.365 \, \text{Ra}^{0.213} \tag{3c}$$

The exponents in Eq. 3 are closer to laminar than to turbulent free convection.

Tang and Owen [11] developed a theoretical model for the closed cavity case, assuming that the heat transfer from the cylindrical surfaces were equivalent to laminar free convection from a horizontal plate but with the gravitational acceleration replaced by the local centripetal acceleration. In addition, they assumed that adiabatic compressible flow occurred in the fluid core between the thermal layers on the rotating cylindrical surfaces. There was generally good agreement between the theoretical and experimental Nusselt numbers for 194 experiments in the three different cavities of Bohn *et al* [9]. The flow appeared to remain laminar at values of Gr normally associated with turbulent flow for stationary plates; this was consistent with the results of experiments conducted in open rotating cavities. Note that large Coriolis forces will suppress turbulence in the fluid core and the differences between the rotational speed of the core (near solid-body rotation) and the discs is relatively small. They showed that compressibility of the cavity air was the reason why the exponents in Eq. 3 were less than ¼, the value associated with laminar free convection.

Sun *et al.* [12] solved the three-dimensional, unsteady compressible Navier-Stokes equations for cavity B in Bohn *et al.* [9]. This was without Reynolds averaging and turbulence modelling. Cavity segments of 45° and 360° were modelled, and good agreement was shown between the calculated Nusselt numbers across the range $2\times10^8 <$ Ra $< 10^{10}$.

King *et al.* [13] solved the vorticity-stream form of the two-dimensional, unsteady incompressible Navier-Stokes equations with the Boussinesq approximation for the same cavity. They found between four and six pairs of large-scale counter-rotating vortices, with

their number varying with time. The computed Nusselt numbers were higher than the measured values but in agreement with correlations for stationary cavities [14,15].

Pitz *et al.* [16] simulated the flow in the same closed cavity using a three-dimensional. incompressible direct numerical simulation (DNS) with the Boussinesq approximation. The results showed that there were four pairs of counter-rotating vortices at $Ra = 10^8$ and five at $Ra = 10^7$. They demonstrated that the flow structures could drift in the same or the opposite direction of the rotation, depending on the values of Ra. The calculated Nusselt numbers using the conventional Boussinesq approximation were higher than those measured by Bohn *et al.* [9] but in good agreement with the correlations in Holland *et al.* [14].

Pitz *et al.* [17] conducted a linear stability analysis and DNS for the flow in closed cavities with various values of *a*/*b*. They obtained the critical number of vortex pairs, which was in agreement with Eq. 1. They also showed that the presence of the discs allowed the flow structure to drift relative to the rotating frame. The same authors presented the calculated velocity profiles in the boundary layers on the adiabatic discs, using three-dimensional, incompressible large eddy simulation (LES) with the Boussinesq approximation [18]. The behavior of the instantaneous velocity profiles aligned with those of laminar Ekman layers.

Saini *et al.* [19] used a three-dimensional compressible DNS solver to study the flow in cavity B for $10^6 < Ra < 10^8$. The number of counter-rotating vortices varied with Ra and the calculated Nusselt numbers were lower than those from the incompressible DNS by Pitz *et al.* [16].

Gao *et al.* [20] compared Nusselt numbers and velocity profiles of disc boundary layers calculated from three-dimensional incompressible DNS and compressible LES

codes for the same cavity. Both codes confirmed the laminar Ekman layer behavior for the

cases considered ($10^7 < Ra < 10^9$). The computed Nusselt numbers were higher than the

measured values in [9], but the exponent of the Nu-Ra correlation from the LES results

(0.286) agreed well with the corrected experimental exponent provided by Bohn and Gier

[21] (0.297). A similar exponent was obtained by Saini and Sandberg [22] using a

compressible DNS solver.

As far as the authors are aware, the most recent set of experimental data generated by

a heated, closed rotating cavity rig were those presented by Bohn *et. al* [9]. This paper

presents radial distributions of disc temperature and heat flux for the first time. In addition,

the flow structures in the core were detected by unsteady pressure measurements, which

are the first of their kind in a closed cavity. These results will be of practical interest to

engine designers for the refinement of design codes, and for the validation of computational

models. Shroud heat transfer results are not presented here, as this would involve the

measurement or calculation of the core temperature, which is beyond the scope of this

paper.

3. BATH COMPRESSOR-CAVITY RIG

Experiments were conducted using the Bath Compressor-Cavity Rig, which simulates

the engine at fluid-dynamically scaled conditions. The design features of the rig are

explained in detail by Luberti *et al.* [23]. A brief overview of the instrumentation and the

experimental range of operation is provided here.

An isometric view of the rig is presented in Fig. 3, and the main dimensions of the test

section are shown in Fig. 4. Note $a/b = 0.45$. The disc drum was mounted on a spindle,

which was driven via a belt by a 30 kW motor. The rig can achieve rotational speeds in the

range $800 < N < 8{,}000$ rpm ($3\text{x}10^5 < \text{Re}_\phi < 3\text{x}10^6$), which were measured by a motor encoder to within ± 10 rpm. An extraction unit drew cool, ambient air through a bell-mouth inlet at the front of the disc drum, and the air flowed axially between the bore of the discs and a stationary central shaft. This flow of air provided the necessary heat sink to cool the inner cylindrical surface of the closed cavity. For these experiments, the flow rate was fixed at approximately 0.1 kg/s, with a measurement accuracy of $\pm 0.5\%$.

The disc drum contained three cavities. For the closed cavity experiments in this paper, aluminum rings (highlighted red in Fig. 3) were attached to the cobs. To minimize the thermal resistance, thermal grease was applied to the mating surface of the rings. The transfer of heat and mass between the axial cooling flow and the outer cavities was prevented by annular Rohacell inserts. The heat transfer and unsteady pressures were measured in the central cavity.

The back surfaces of the central and outer discs were insulated with Rohacell, a low thermal conductivity foam, which provided a near-adiabatic condition for the back surfaces of the central discs. The front (cavity-side) surfaces of the discs, shroud and hub were painted with matt black paint. As explained below, this enabled the heat flux measurements to be corrected for radiation. (Although black paint increases the radiation, it makes it possible to compute with greater certainty.)

The temperature of the shroud was controlled by a set of six 2 kW circular heater elements. These enabled the shroud to achieve temperatures in excess of 100 °C and the buoyancy parameter to reach $\beta \Delta T \sim 0.15$.
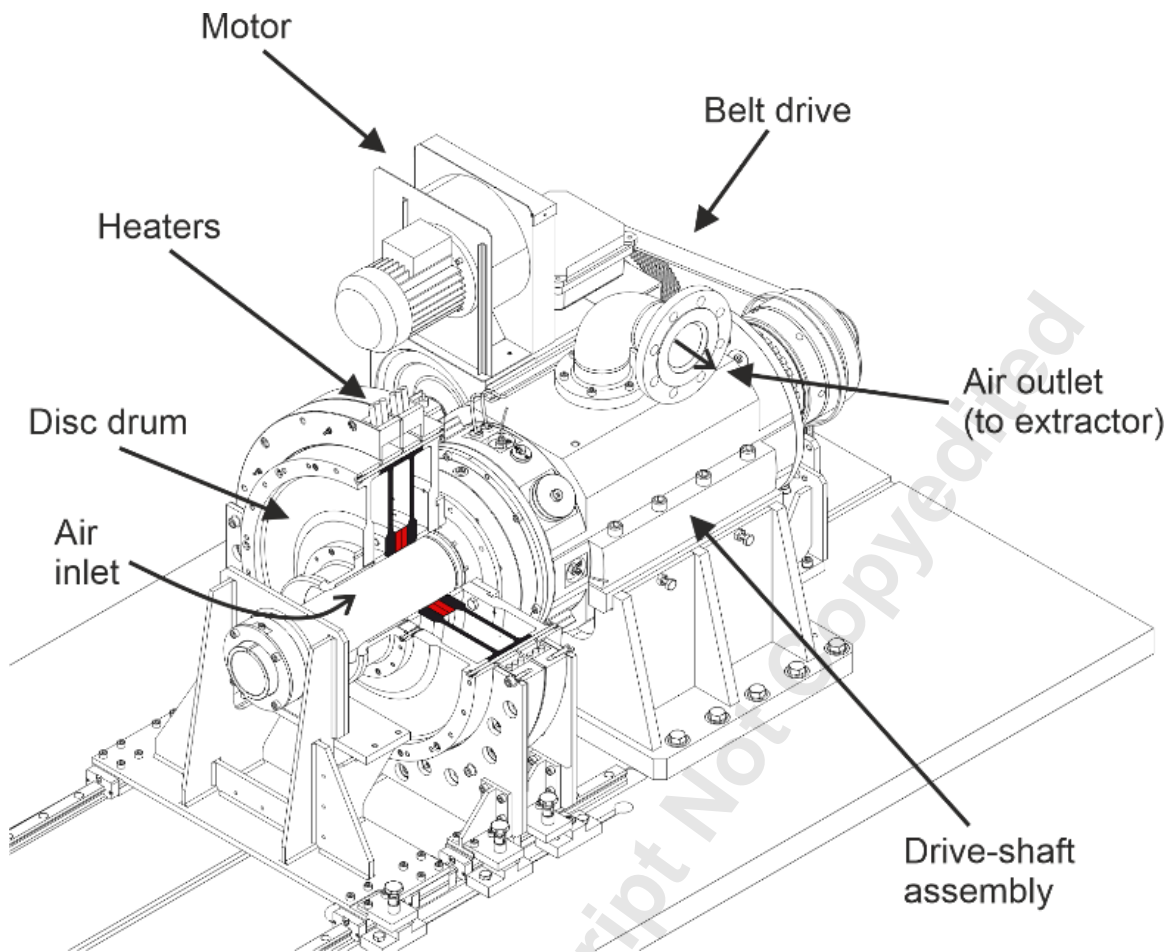
Figure 3: The experimental rig showing a section view of the disc drum. The central cavity test section is shaded black and the aluminum rings are shaded red.

Figure 4 shows the instrumented central cavity and axial flow annulus. The rotating

surfaces of the discs were instrumented with 64 thermocouples. On the radial surfaces of

the diaphragm and cob, K-type thermocouples were directly embedded in circumferential

grooves in the disc surface using epoxy cement to minimize thermal disturbance errors.

Thin foil thermocouples and fluxmeters (see [24]) were attached on the underside surfaces

of the shroud. However, no results are presented for heat transfer from the shroud, as this

would involve the measurement or calculation of the core temperature, which is beyond

the scope of this paper. The temperature of the axial flow measured using two rakes that

were mounted on the stationary shaft. Each rake contained five evenly spaced K-Type
thermocouples. The shaft temperature was also measured at the same axial position as both
rakes.
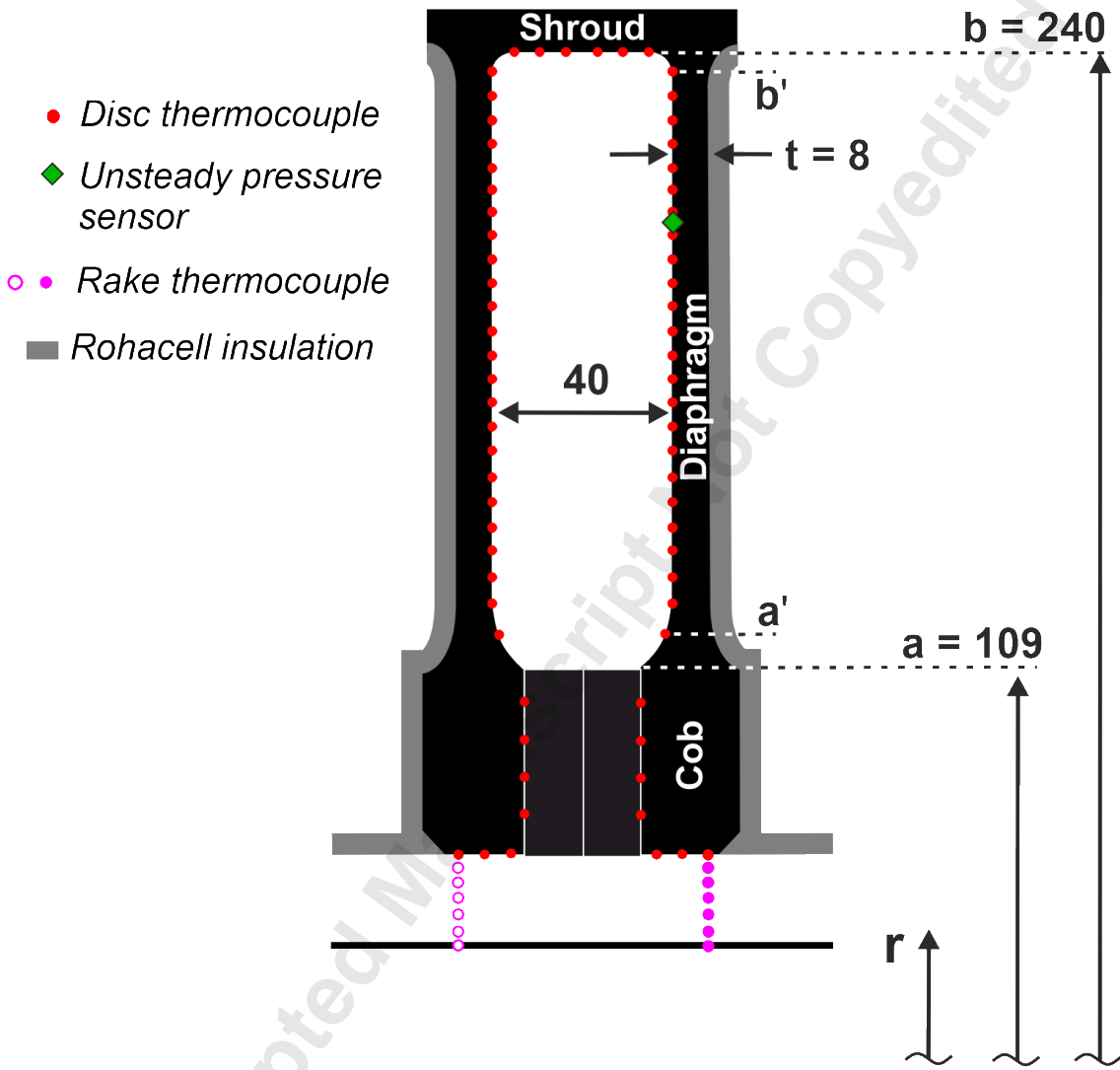
Figure 4: Cross-section of the central cavity, showing disc and rake thermocouple locations and the unsteady pressure sensors on the disc. The main dimensions are given in millimeters.

Two fast-response unsteady pressure sensors (Kulite XCQ-080 series) were used to determine the number of vortex pairs and the slip of these structures. The transducers were mounted flush to the diaphragm of the downstream disc of the cavity at a radius ratio of $r/b = 0.85$. The circumferential spacing of the sensors was $\alpha = 35°$.

The wires from the rotating instrumentation passed through the center of the spindle to a Datatel telemetry unit. The thermocouples were pinned into the sockets of four transmitter modules, each of which contained a PT100 Resistance Temperature Detector (RTD) to provide the cold-junction compensation for that module. The fast-response pressure sensors were connected to a separate high-frequency transmitter module. The estimated combined uncertainty of the rotating thermocouples is described by a standard deviation of ± 0.5 °C.

The data from the pressure sensors passed through a 1 kHz low-pass filter before being sampled at 10 kHz to minimize effects of signal aliasing. For each test, a 100 s sample was collected (10^6 sample points). At the maximum rotational speed of these experiments, 8,000 rpm, the disc frequency was $f_d = 133$ Hz. The measured rotational frequency of the structures was lower (around $0.02f_d$ – see Section 5), as the sensors collected pressure measurements in the *rotating frame* of reference. Therefore, the frequency of the low-pass filter was sufficiently high to satisfy the Nyquist criterion. A National Instruments NI 9215 data logger was used to acquire the pressure data. The combined uncertainty of the absolute pressure measurement, described by the standard deviation, is ± 1.5 mbar.

The static and rotating thermocouple measurements were sampled at 10 Hz. A non-dimensional temperature based on the axial cooling flow, Θ_f, was used to assess whether a steady-state condition had been reached:

$$\Theta_f = \frac{T_o - T_f}{T_{o,b'} - T_f} \tag{4}$$

Conditions were considered to be steady-state if the median average of Θ_f for each disc

thermocouple changed by less than 0.01 between a pair of 10 minute intervals.

In total, 11 experiments were conducted across a range of $\beta\Delta T$ and Re_ϕ (and therefore,

Gr). These parameters are defined in the nomenclature. Table 1 presents the dimensional

and non-dimensional parameter ranges for the experiments.

a)

Parameter	N [rpm]	ΔT [°C]	$\dot{m}$ [kg/s]
Range	2,000 – 8,000	21 - 47	~ 0.1

b)

Parameter	$\beta\Delta T$	Re_ϕ (x10^6)	Gr (x10^{11})
Range	0.07 - 0.15	0.8 – 2.8	0.4 – 9.3

Table 1: Dimensional (a) and non-dimensional (b) experimental parameter ranges.

4. DISC HEAT TRANSFER

4.1 Measurement and analysis of experimental data

The radial distribution of the disc temperature is shown in Fig. 5a for an example case.

Figure 5b shows the equivalent non-dimensional temperature, Θ:

$$\Theta = \frac{T_o - T_{o,a'}}{T_{o,b'} - T_{o,a'}} \tag{5}$$

The measurement locations are indicated on the silhouette of the central cavity, which

are radially aligned with the figures either side. The axial flow is from left to right. The

axial flow rake and shaft temperatures upstream and downstream of the cavity are also

shown.

The radial distribution of temperature for the upstream and downstream discs is equal within experimental uncertainty, indicating similar heat transfer between each disc and the cavity air. There is a slight temperature rise of the axial flow, due to the transfer of heat from the hotter cobs and ring attachments. Figure 5b shows that the temperature here is very similar between both discs and along the radial coordinate, indicating good conduction within the rings themselves and across the mating interface.
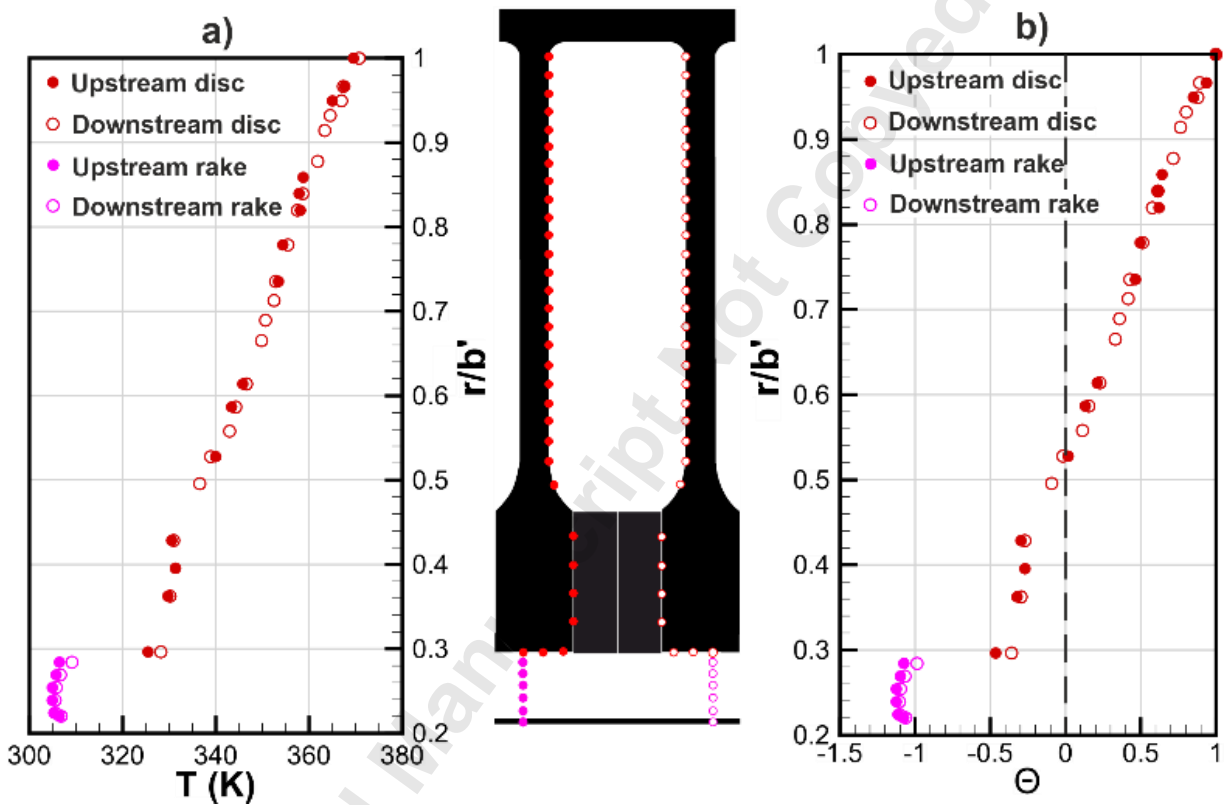

Figure 5: Raw temperatures (a) and non-dimensional temperatures (b) on the upstream and downstream disc, for an example case (Re$_\phi$ = 2.6x10^6, $\beta\Delta T$ = 0.14, Gr = 9.3x10^{11}).

A Bayesian statistical model used in conjunction with a circular fin model for conduction in the discs (see [8]) was used to derive the heat flux distribution from the measured disc temperatures. An explanation of how these models were used for the

analysis of experimental data from the Bath rig is given by Jackson *et al.* [3]. The input to

the models is the average temperature of the discs at each discrete radial coordinate. The

Bayesian model uses these temperatures, together with the fin equation, to calculate the

optimized solution for the radial distribution of disc temperature and heat flux.

Figure 6a shows the measured values of Θ together with the continuous distribution

derived from the Bayesian model. The 95% confidence interval is also shown by the grey

fill. The corresponding heat flux distribution is shown in Fig. 6b and is consistent with the

buoyancy-induced flow described in Section 1. A positive flux indicates that heat is

transferred from the disc to the air (*i.e.* the disc is hotter than the adjacent cavity air), while

negative suggests that the reverse occurs (*i.e.* the disc is colder than the air).

The Bayesian model calculates the *total* heat flux (combined convective and radiative

fluxes). A radiation model (see [25]) was used to calculate the radiative heat fluxes from

or to the disc surfaces, and the total flux was corrected to produce the radial distribution of

convective flux in Fig. 7. The radiative component is marked as the red line. The disc

surfaces at $r/b' > 0.98$ (where radiative heat flux is positive) lose heat due to radiation,

while surfaces elsewhere gain heat. For the case presented in Fig. 7, the radiation

component is 3% of the total heat flux at $r/b' = 1$, and 14% of the total at $r/b' = 0.52$. Of

the experimental conditions tested, the radiation can be up to 5% of the total heat flux at

$r/b' = 1$, and 25% of the total at $r/b' = 0.52$.
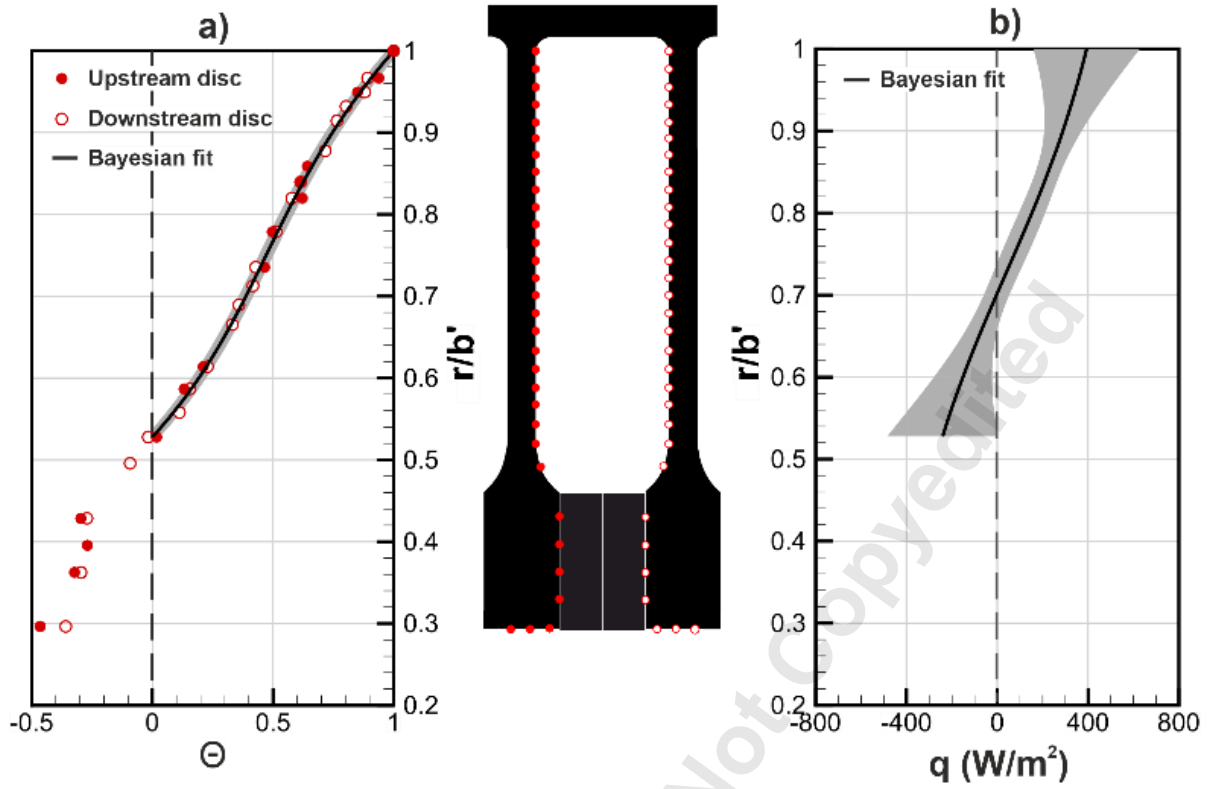
Figure 6: Radial distribution and uncertainties of Θ (a) and q (b) calculated from

**the Bayesian model ($\mathrm{Re}_\phi = 2.6\mathrm{x}10^6$, $\beta\Delta T = 0.14$, $\mathrm{Gr} = 9.3\mathrm{x}10^{11}$).**
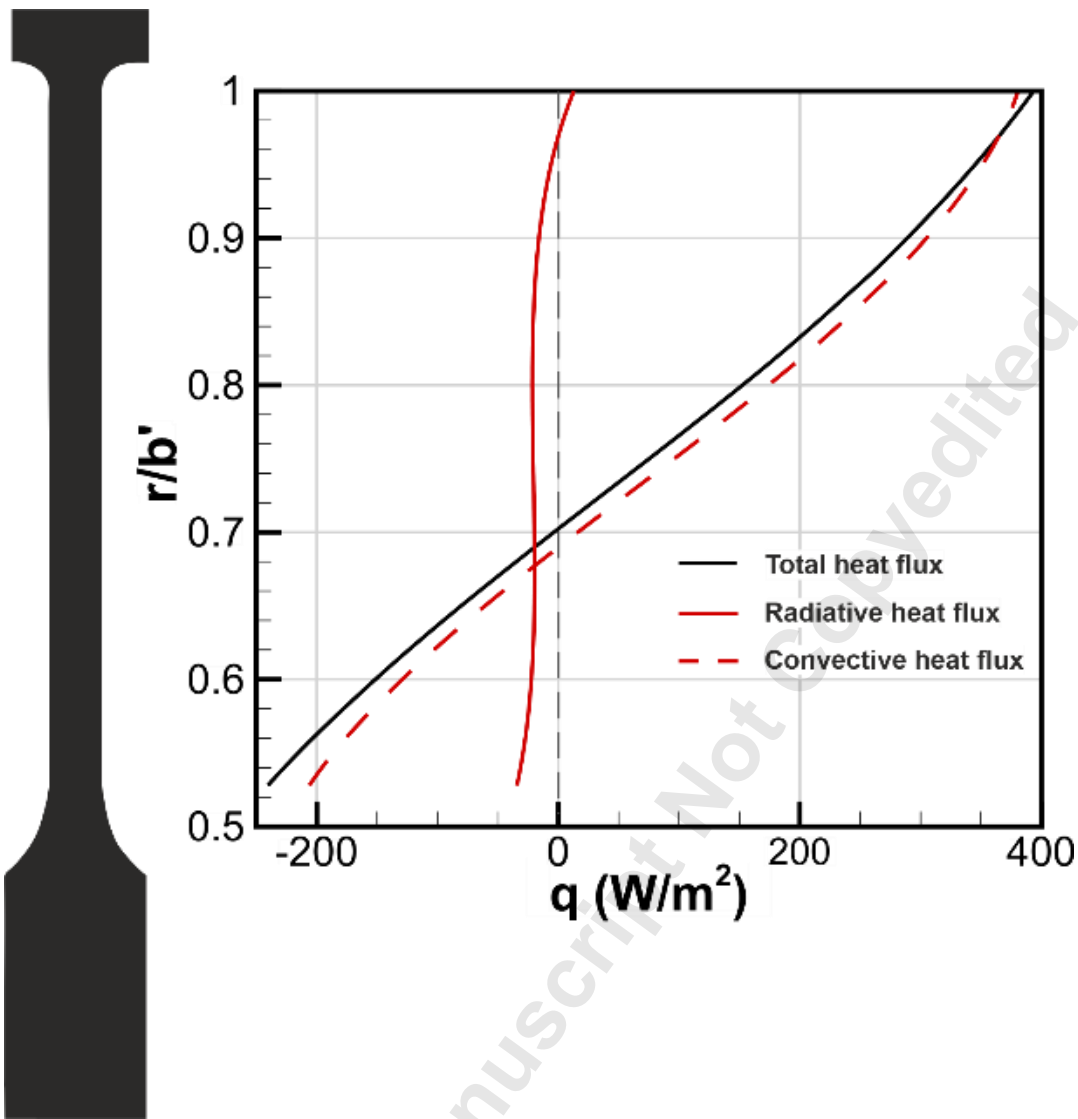
Figure 7: Effect of radiation on radial distribution of heat flux (Re$_\phi$ = 2.6x10^6, $\beta\Delta T$ = 0.14, Gr = 9.3x10^{11}).

4.2 Discussion of disc temperatures and heat fluxes

Figure 8a shows the radial distribution of Θ for the lowest speed tested ($N = 2000$ rpm, Re$_\phi \sim 0.7$x10^6) for three values of $\beta\Delta T$. At this low speed, there is a remarkable collapse of the data onto virtually a single curve showing that the effect of $\beta\Delta T$ is negligible. Figure 8b shows the radial distribution of Θ over a range of rotational speeds for a common value of $\beta\Delta T = 0.11$. Though subsumed by the margin of experimental uncertainty, there is a

small, monotonic departure from this common curve with increasing Reynolds number; this is attributed to compressibility effects, as found in open rotating cavities, where the core temperature increases as the rotational speed increases (see [26]). Figure 8c shows all the radial distributions of Θ plotted on the same axes. This illustrates that, over a wide range of parameters, the radial variation of Θ is not significantly affected by the values of $\beta\Delta T$ and Re_ϕ.

As this is a conjugate problem, where the equations for the temperatures of the disc and core are coupled, the above distributions imply that the solution of these equations is unique if compressibility effects are negligible: there is only one possible radial distribution of nondimensional disc temperature for any particular closed cavity. *As the temperature distribution depends on conduction in the disc, it will therefore depend only on the particular cavity geometry and the thermal properties of the disc material.*
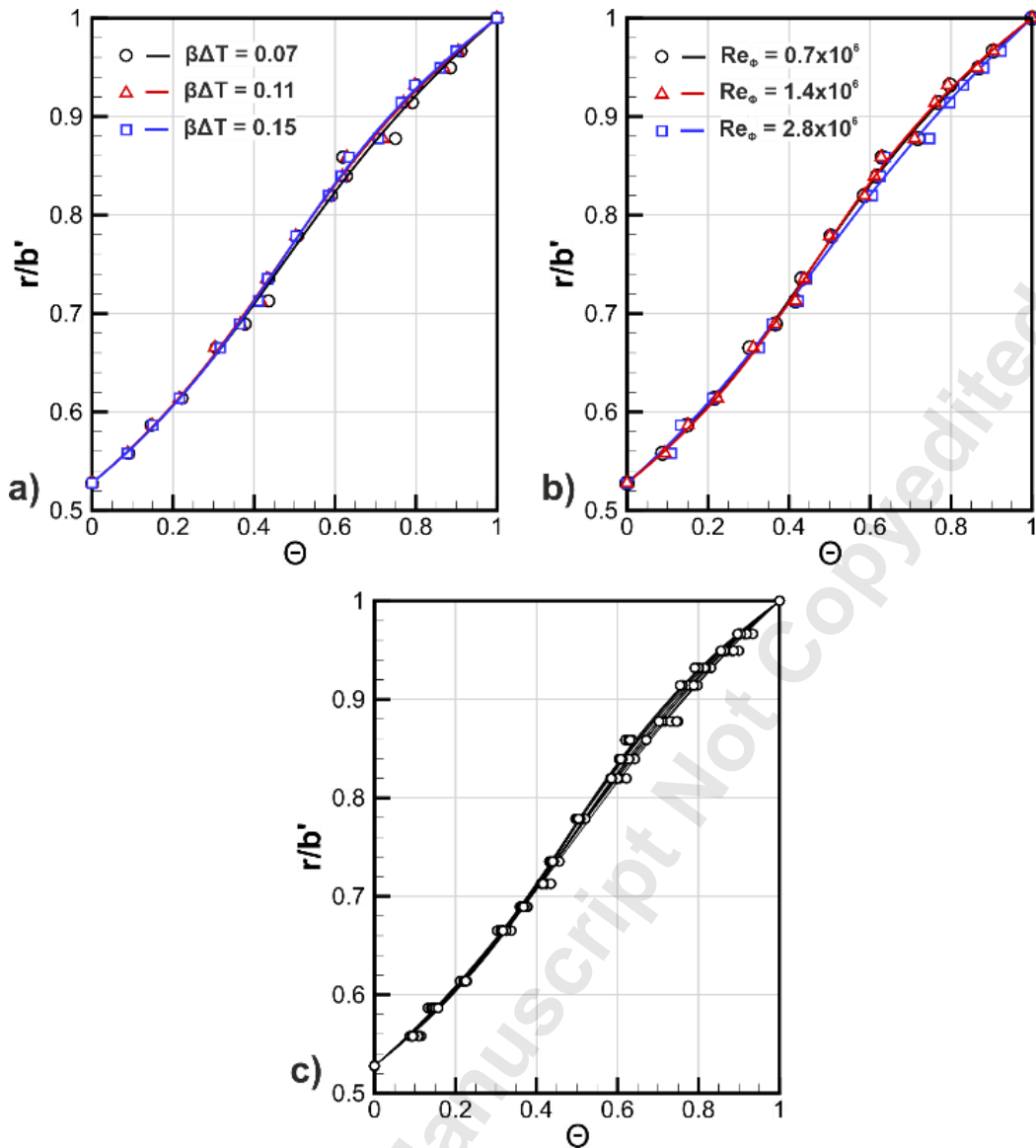
Figure 8: Radial distributions of Θ, showing effect of $\beta\Delta T$ at $Re_\phi = 0.7\text{x}10^6$ (a), effect

of Re_ϕ at $\beta\Delta T = 0.11$ (b) and a comparison of all 11 test cases (c).

Figure 9 shows the radial distribution of the *convective* heat flux for the 11 test cases.

As discussed in Section 1, the flux is positive for the larger radii and negative for the

smaller values. Of particular note is that the radial location of the crossover from positive

to negative flux is virtually the same, where $r/b \sim 0.7$, for all 11 sets of data. This implies

that at this crossover radius (r* say) where the flux is zero, the temperatures of the disc and

core must be equal. For $r > r*$, the disc is hotter than the core, and *vice versa* for $r < r*$.

The near-uniqueness of the value of $r*/b$ is consistent with the near-uniqueness of the

temperature distributions discussed above.
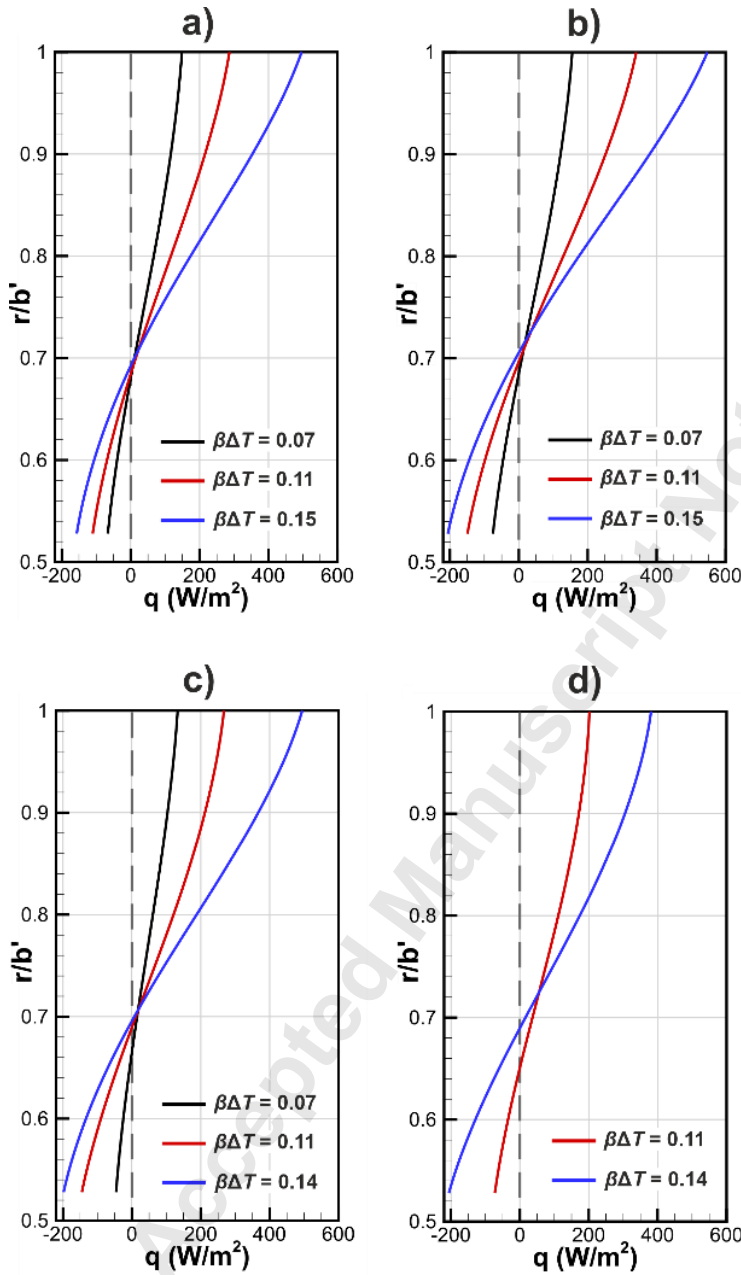
Figure 9: Effect of *βΔT* on the radial distribution of convective heat flux, *q*, for Re$_\phi$ ~

0.7x10^6 (a), Re$_\phi$ ~ 1.4x10^6 (b), Re$_\phi$ ~ 2.1x10^6 (c) and Re$_\phi$ ~ 2.7x10^6 (d) .

The *dimensional* flux distributions - which show that the magnitude of the flux increases as $\beta \Delta T$ increases - are obviously not unique. The flux depends on the difference between the temperatures of the disc and core; as the latter is unknown a *meaningful* Nusselt number could not be calculated.

The radially-weighted average heat flux, $\bar{q}$, is defined as:

$$\bar{q} = 2 \frac{\int_{a'}^{b'} q r \, \mathrm{d}r}{\left(b'^2 - a'^2\right)} \tag{6}$$

Figure 10 illustrates the effect of $\beta \Delta T$ and Re_ϕ on the variation of $\bar{q}$ with Grashof number, Gr. For fixed rotational speed, $\bar{q}$ increases with increasing $\beta \Delta T$ due to the stronger buoyancy forces driving the convection. With increasing Re_ϕ, $\bar{q}$ initially increases but the temperature of the core also increases due to compressibility effects. Therefore, there is a critical value of Re_ϕ beyond which the heat transfer reduces. This effect is apparent by the reduction in $\bar{q}$ at $Re_\phi = 2.7 \times 10^6$ for both values of $\beta \Delta T$. The corresponding radial distributions of q in Fig. 9d shows a reduction in the magnitude of positive q when compared to the equivalent distributions in Fig. 9c. A similar phenomenon was observed by Jackson *et al.* [3] for the open cavity case.

No results are presented for heat transfer from the shroud as this would involve the measurement or calculation of the core temperature, which is beyond the scope of this paper.
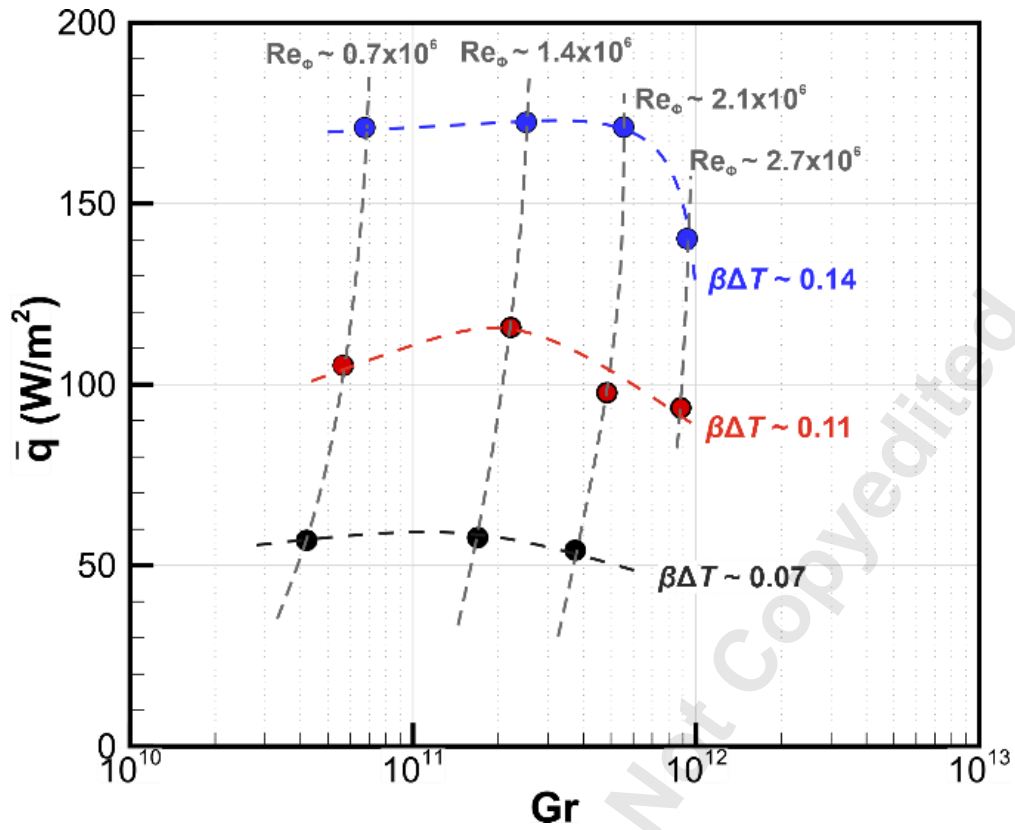
Figure 10: Effect of $\beta\Delta T$ on variation of radially-weighted average disc heat flux

with Gr.

5. UNSTEADY PRESSURE MEASUREMENTS

For the tests reported here, the two pressure sensors were mounted at a radius ratio of

$r/b = 0.85$ and a circumferential spacing of $\alpha = 35°$.

Figure 11 shows a schematic of the flow structure in the closed cavity for an example

with three vortex pairs. The angular speed of the discs is Ω and the structures rotate about

the z axis at a speed of Ω_s, which can be determined as follows:

$$\Omega_s = \frac{\alpha}{\Delta t_\alpha} \tag{7}$$
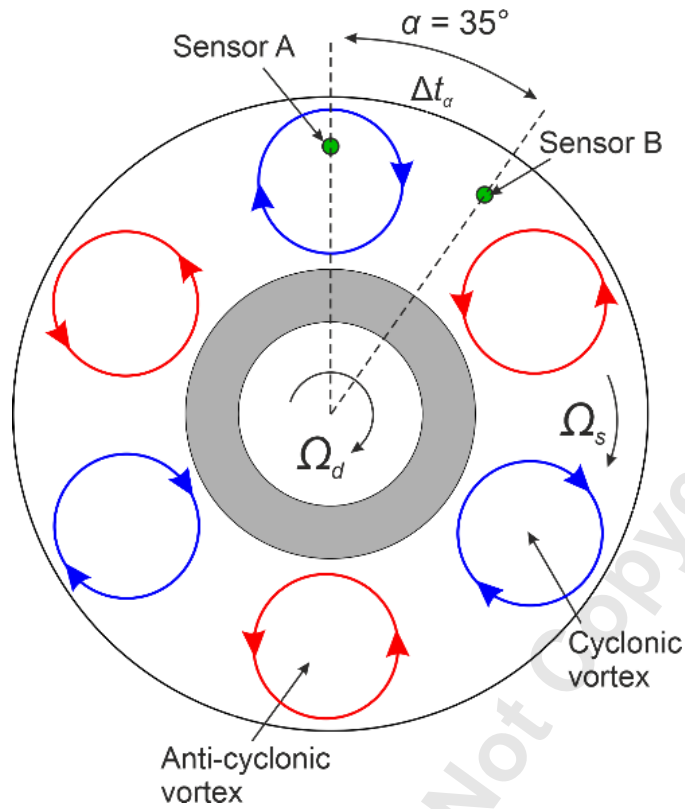
Figure 11: An example flow structure in the r-ϕ plane of the closed cavity, showing three vortex pairs. The shaded grey area denotes the cob attachments.

Using the same technique as described by Jackson *et al.* [7], the time lag between Sensors A and B, Δt_α, can be found from the peak of the cross-correlation between the two signals, as can whether $\Omega_s < \Omega$, or vice versa. This is discussed in more detail below. The number of vortex pairs, n, can then be deduced from:

$$n = \frac{2\pi f_{s,1}}{\Omega_s} \tag{8}$$

where $f_{s,1}$ is the passing frequency of one vortex pair, found from the fast Fourier transform (FFT) of the signal from either sensor.   Figure 12 presents the FFT results, expressing the frequency as a function of the disc rotational frequency, f_d. The pressure coefficient, C_p, is

GTP-21-1400   Jackson   25

defined from the difference between the static pressure, p, and the mean of the data sample, $\bar{p}$:

$$C_p = \frac{p - \bar{p}}{0.5 \rho_f \Omega^2 b^2} \tag{9}$$

The measured passing frequency of a single vortex pair, $f_{s,1}$, is shown by the peaks in Fig. 12 and approximately 2 - 3% of the disc frequency. It is important to note that this is not equivalent to the rotational frequency of the core, which will depend upon the number of vortex pairs – this is discussed below.
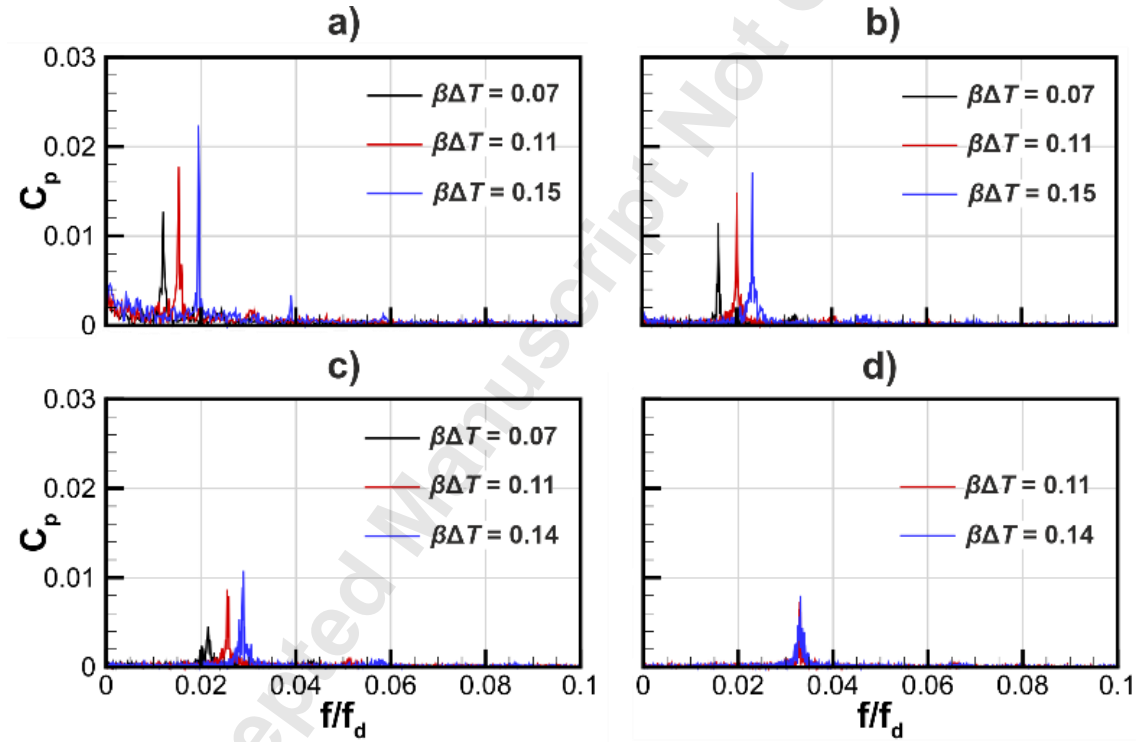
Figure 12: Effect of $\beta\Delta T$ on the frequency spectra of the pressure measurements for $Re_\phi \sim 0.7\times10^6$ (a), $Re_\phi \sim 1.4\times10^6$ (b), $Re_\phi \sim 2.1\times10^6$ (c) and $Re_\phi \sim 2.7\times10^6$ (d). Results shown for Sensor A.

The cross-correlation of the data from both sensors is necessary to determine whether the structures are rotating faster or slower than the discs. This is expressed as $p_A(t) \star p_B(t+\Delta t)$, where Δt is the time lag. The peak of the cross-correlation will occur when $\Delta t = \Delta t_\alpha$. Therefore, if the correlation peaks at a positive value of Δt_α, then Sensor B has sensed the structures before Sensor A, and so the structures are rotating slower than the disc, and vice versa.

Figure 13 shows the cross-correlation of two example cases (one at $N = 6,000$ rpm and a second at $N = 8,000$ rpm), normalized with respect to the maximum correlation value. The abscissa is shown as a function of Δt, expressing the circumferential angle which the structures have covered in time Δt. It follows that the cross-correlation will peak at α, where, by definition, $t = \Delta t_\alpha$. At this unique point, through combination and rearrangement of Eqs. 7 and 8:

$$\alpha = \frac{2\pi f_{s,1} \Delta t_\alpha}{n} \tag{10}$$

Since the cross-correlation must peak where $\Delta t = \Delta t_\alpha$, which corresponds with the core rotating by $\phi = \alpha$, n is adjusted until the peak of the cross-correlation coincides with α. Using this analysis, it has been shown that for all experimental cases tested in this study, $\Delta t_\alpha > 0$, meaning that the structures are rotating slower than the disc. *This does not necessarily mean that the fluid core is rotating slower than the discs.* As the pairs of vortices pass a reference point on the disc, the relative velocity of the fluid will oscillate with time. If, as appeared to be the case in the experiments reported here, the vortices in every pair had the same size and strength, albeit with contra rotation, then the time average of the relative fluid velocity would equal that of the core. This would not necessarily be the case if the vortices did not have the same size and strength.

GTP-21-1400   Jackson   27

The second observation from Fig. 13 is that for the $N = 6,000$ rpm case (Fig. 13a), there are shown to be three vortex pairs, while for the $N = 8,000$ rpm case (Fig. 13b), there are four pairs. Of the experimental conditions tested, three vortex pairs were detected at rotational speeds $N < 8,000$ rpm for all values of $\beta\Delta T$, while four pairs were only detected for the $N = 8,000$ rpm cases. (A value of $n = 4$ in Eq. 1 is consistent with $a/b = 0.44$, which is close to the radius ratio of this cavity.) Computationalists have shown that the number of vortex pairs can change with Gr [13, 16, 19], but this is the first time it has been demonstrated experimentally for a closed cavity.

Contour plots and ensemble averages of C_p are presented in Fig. 14 for the two example cases previously shown in Fig. 13. The contour plots show the circumferential variation of pressure coefficient along the ordinate (in the frame of reference of the structures) with the number of complete structure revolutions along the abscissa. The data reveal periods where the vortices precess faster and slower than the dominant rotational frequency, f_s. An ensemble average is shown for both cases across ten structure revolutions where the rotational speed of the structures is stable; the vertical dashed black lines indicate the limits across which they are averaged. These ensemble averages confirm that the vortices precess about the abscissa slower than the discs rotate, as the pressure signal from Sensor A lags Sensor B. The averages also reveal the similarity of size and strength of each vortex pair. As stated above, this implies that the angular speed of the vortices is equal to that of the core. It also explains why only a single dominant peak is shown in the FFT. The magnitude of the pressure in the ensemble average is greater than the FFT, as the FFT considers the whole pressure sample. The variation in the rotational speed of the vortices creates a smearing effect in the pressure magnitude of the FFT in Fig. 12.
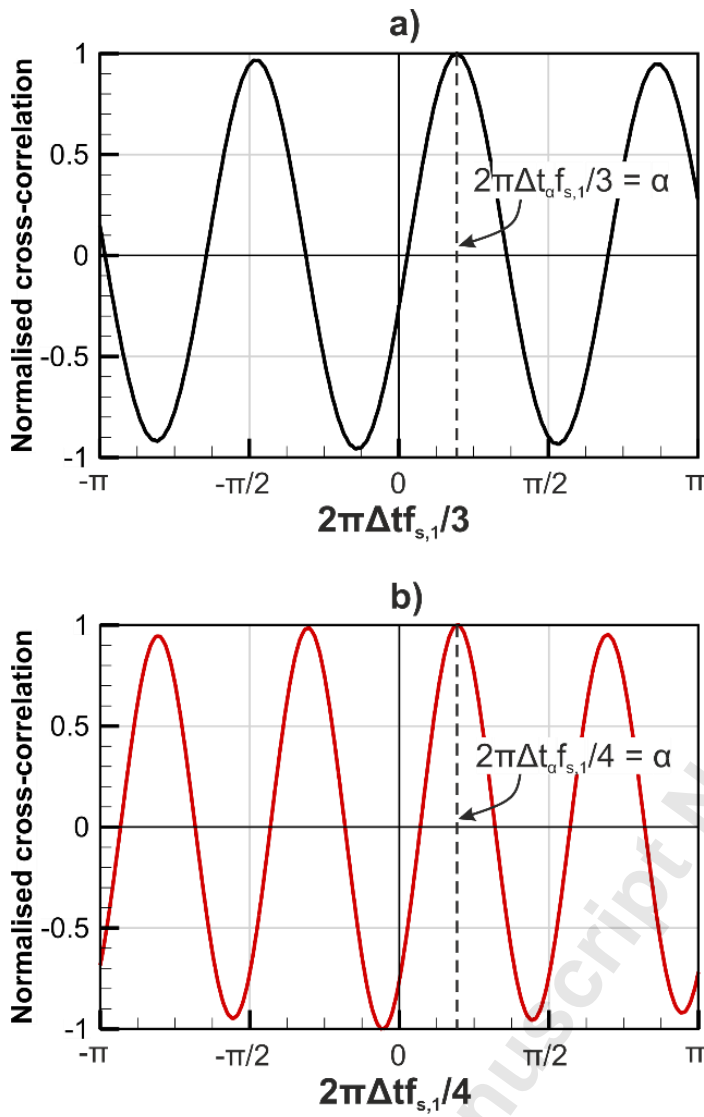
Figure 13: Example cross-correlation results for $Re_\phi = 1.3 \times 10^6$ (a) and $Re_\phi = 2.6 \times 10^6$

(b) ($\beta \Delta T \sim 0.14$).
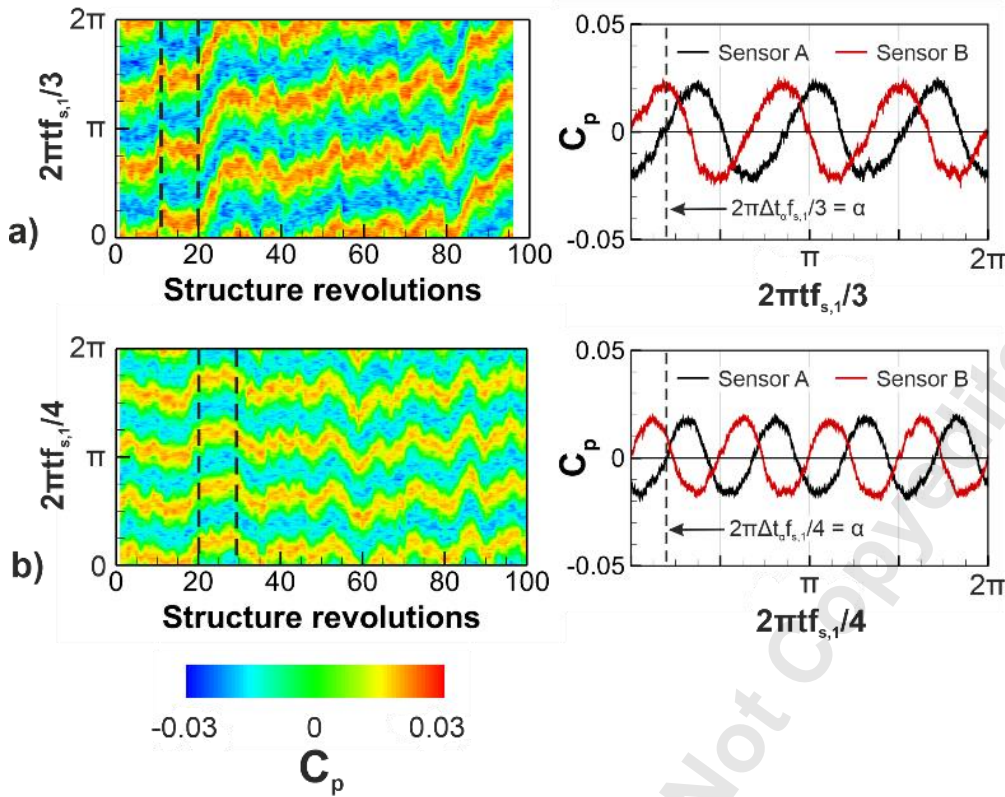
Figure 14: Contour plots of C_p and corresponding ensemble averages over the stable

region marked by the black dashed lines. $Re_\phi = 1.4 \times 10^6$ (a) and $Re_\phi = 2.6 \times 10^6$ (b)

($\beta \Delta T = 0.14$ for both).

Figure 12 can be reviewed using this new understanding. For most values of Re_ϕ (Re_ϕ

~ 2.7×10^6 – Fig. 12d), the slip of the structures, and hence that of the core, increases with

$\beta \Delta T$ and Gr. Similarly, with an increase in $\beta \Delta T$, the magnitude of C_p generally increases,

indicating the strengthening of the vortices.

Following identification of the number of vortex pairs, the rotational frequency of the

entire flow structure, f_s, can be found from $f_s = f_{s,1}/n$. Applying this to the results in Fig. 12,

reveals that the difference between the disc and core rotation is less than 1% of the disc

speed for the cases considered. In other words, the fluid experiences almost solid body

rotation.

6. CONCLUSIONS

Disc temperature and unsteady pressure measurements were collected from a closed cavity (with $a/b = 0.45$) of the Bath Compressor-Cavity Rig over a range of engine representative conditions. The corresponding ranges of non-dimensional parameters were $0.07 < \beta\Delta T < 0.15$; $0.8\text{x}10^6 < \text{Re}_\phi < 2.8\text{x}10^6$; $0.4\text{x}10^{11} < \text{Gr} < 9.3\text{x}10^{11}$. Radial distributions of the total disc heat flux were derived from the temperature measurements using Bayesian statistics, together with the conduction equations for a circular fin. A radiation correction was used to separate the convective heat flux from the total. The measured disc temperatures and heat fluxes are the first to be published.

For the 11 cases tested, the radial variation of Θ, the nondimensional disc temperature, was mainly unaffected by the variation of $\beta\Delta T$ or Re_ϕ. There was a minor, monotonic influence of increasing Reynolds number, attributed to compressibility effects where the core temperature increases as the rotational speed increases. That is, if compressibility effects are negligible,

the radial variation of Θ would be unique. This suggests that *all* rotating closed cavities should have a disc temperature distribution dependent only on the geometry and disc material of the cavity. The influence of compressibility is minor, even at engine conditions, and so the important discovery of a unique temperature distribution will be of practical use to the engine designer and will simplify thermo-mechanical modelling.

In all tests, the disc heat flux was positive for the larger radii and negative for the smaller values. The radial location of the crossover from positive to negative flux, where $r/b \sim 0.7$, was virtually the same for all sets of data, and indeed unique within experimental certainty when compressibility effects were negligible. As this is a conjugate problem,

where the equations for the temperatures of the disc and core are coupled, the common crossover point is consistent with the unique disc temperature distribution.

There was a critical value of Re_ϕ above which the radially-weighted average disc heat flux decreased with increasing Re_ϕ. This decrease was attributed to compressibility effects, as found in open cavities.

The unsteady pressure sensors, located at $r/b = 0.85$, detected between three and four vortex pairs across the range of experimental conditions. This is consistent with the number of vortex pairs predicted from the circular-vortex hypothesis. The number of pairs changed with Gr, and the fluid core slipped relative to the discs by less than 1% of the disc speed.

ACKNOWLEDGEMENTS

NOMENCLATURE

a	inner radius of cavity (hub) [m]
a'	radius of innermost thermocouple on disc diaphragm [m]
b	outer radius of cavity (shroud) [m]
b'	radius of outermost thermocouple on disc diaphragm [m]
f_d	rotational frequency of discs [Hz]
$f_{s,1}$	passing frequency of one vortex pair [Hz]

n	number of vortex pairs	
N	rotational speed of discs [rpm]	
p	static pressure [Pa]	
$\bar{p}$	mean static pressure [Pa]	
q	heat flux [W/m^2]	
$\bar{q}$	radially-weighted average heat flux [W/m^2]	
r	radius [m]	
r_s	outer radius of shaft [m]	
s	cavity width [m]	
t	time [s]	
T	temperature [K]	
α	angular separation of unsteady pressure sensors [rad]	
β	volume expansion coefficient [K^{-1}]	
ρ	density [kg/m^3]	
μ	dynamic viscosity [m^2/s]	
Δt	time lag between unsteady pressure sensors [s]	
Ω	angular velocity of disc [rad/s]	
Ω_s	angular velocity of rotating structures [rad/s]	

Dimensionless parameters

C_p	Pressure coefficient $(= (p - \bar{p})/(0.5\rho_f\Omega^2 b^2))$	
Gr	Grashof number $(= \mathrm{Re}_\phi^2\beta\Delta T)$	
Ra	Rayleigh number	
Re_ϕ	rotational Reynolds number $(= \rho_c\Omega b^2/\mu_f)$	
$\beta\Delta T$	buoyancy parameter $(= (T_{o,b} - T_{o,c})/T_{o,c})$	

Θ non-dimensional temperature ($= (T - T_{o,a'})/(T_{o,b'} - T_{o,a'})$)

Subscripts

A, B value from pressure sensor A, B

$a;\ a';\ b;\ b'$ values at $r = a$; $r = a'$; $r = b$; $r = b'$

c average value on radial cob surface

o value on disc surface

f value in axial cooling flow

ϕ,r,z circumferential, radial and axial direction

REFERENCES

[1] "Cross-section of the SGT6-4000F (V84.3A) gas turbine", last modified 2016, accessed November 26, 2020, https://bit.ly/2J1Yez7

[2] Farthing, P. R., Long, C. A., Owen, J. M., and Pincombe, J. R., 1992, "Rotating Cavity with Axial Throughflow of Cooling Air: Flow Structure," *ASME J. Turbomach.*, **114**(1), pp. 237–246.

[3] Jackson, R., Luberti, D., Tang, H., Pountney, O., Scobie, J., Sangan, C., Owen, J. M., and Lock, G. D., 2020, "Measurement and Analysis of Buoyancy-Induced Heat Transfer in Aero-Engine Compressor Rotors," ASME *J. Eng. Gas Turbines Power*

[4] Owen, J. M., 2010, "Thermodynamic Analysis of Buoyancy-Induced Flow in Rotating Cavities," *ASME J. Turbomach.*, **132**(3), p. 031006.

[5] Owen, J. M., Pincombe, J. R., and Rogers, R. H., 1985, "Source-sink flow inside a rotating cylindrical cavity," *J. Fluid Mech.*, **155**, pp. 233-265.

[6] Jackson, R., Tang, H., Pountney, O., Scobie, J., Sangan, C., Owen, J. M., and Lock, G. D., 2020, "Analysis of Shroud and Disc Heat Transfer in Aero-Engine Compressor Rotors," *ASME J. Eng. Gas Turbines Power*. [Accepted for publication]

[7] Jackson, R., Tang, H., Pountney, O., Scobie, J., Sangan, C., Owen, J. M., and Lock, G. D., 2021, "Unsteady Pressure Measurements in a Heated Rotating Cavity," ASME Paper No. GT2021-59090.

[8] Tang H., Shardlow T., and Owen, J. M., 2015, "Use of Fin Equation to Calculate Nusselt Numbers for Rotating Disks," *ASME J. Turbomach.*, **137**(12), p. 121003.

[9] Bohn, D., Deuker, E., Emunds, R., and Gorzelitz, V., 1995, "Experimental and Theoretical Investigations of Heat Transfer in Closed Gas-Filled Rotating Annuli," *ASME J. Turbomach.*, **117**(1), pp. 175–183.

[10] Owen, J. M., and Long, C. A., 2015, "Review of Buoyancy-Induced Flow in Rotating Cavities," *ASME J. Turbomach.*, **137**(11), p. 111001.

[11] Tang, H., and Owen, J. M., 2018, "Theoretical Model of Buoyancy-Induced Heat Transfer in Closed Compressor Rotors," *ASME J. Eng. Gas Turbines Power*, **140**(3), p. 032605.

[12] Sun, Z., Kifoil, A., Chew, J. W., and Hills, N. J., 2004, "Numerical Simulation of Natural Convection in Stationary and Rotating Cavities," ASME Paper No. GT2004-53528.

[13] King, M. P., Wilson, M., and Owen, J. M., 2007, "Rayleigh-Benard Convection in Open and Closed Rotating Cavities," *ASME J. Eng. Gas Turbines Power*, **129**(2), pp. 305–311.

[14] Holland, K. G. T., Raithby, G. D., and Konicek, L., 1975, "Correlation Equations for Free Convection Heat Transfer in Horizontal Layers of Air and Water," *Int. J. Heat Mass Tran.*, **18**(7–8), pp. 879–884.

[15] Grossmann, S., and Lohse, D., 2000, "Scaling in Thermal Convection: A Unifying Theory," *J. Fluid Mech.*, **407**, pp. 27–56.

[16] Pitz, D. B., Chew, J. W., Marxen, O., and Hills, N. J., 2017a, "Direct Numerical Simulation of Rotating Cavity Flows Using a Spectral Element-Fourier Method," *ASME J. Eng. Gas Turbines Power*, **139**(7), p. 072602.

[17] Pitz, D. B., Marxen, O., and Chew, J. W., 2017b, "Onset of Convection Induced by Centrifugal Buoyancy in a Rotating Cavity," *J. Fluid Mech.*, **826**, pp. 484-502.

[18] Pitz, D. B., Chew, J. W., and Marxen, O., 2019, "Large-Eddy Simulation of Buoyancy-Induced Flow in a Sealed Rotating Cavity," *ASME J. Eng. Gas Turbines Power*, **141**(2), p. 021020.

[19] Saini, D., Cheung, D., and Sandberg, R., 2018, "Direct Numerical Simulations of Centrifugal Buoyancy Induced Flow in a Closed Rotating Cavity," 21st Australasian Fluid Mechanics Conference.

[20] Gao, F., Pitz, D. B., and Chew, J. W., 2020, "Numerical Investigation of Buoyancy-Induced Flow in a Sealed Rapidly Rotating Disc Cavity," *Int J. Heat Mass Tran.*, **147**, p. 118860.

[21] Bohn, D., and Gier, J., 1998, "The Effect of Turbulence on the Heat Transfer in Closed Gas-Filled Rotating Annuli for Different Rayleigh Numbers," in: Proceedings of ASME 1998 International Gas Turbine and Aeroengine Congress and Exhibition, 1998. Paper No. 98-GT-542.

[22] Saini, D., & Sandberg, R. D., 2020, "Simulations of Compressibility Effects in Centrifugal Buoyancy-Induced Flow in a Closed Rotating Cavity. *Int J. Heat Fluid Flow*, **85**, p. 108656.

[23] Luberti, D., Patinios, M., Jackson, R., Tang, H., Pountney, O., Scobie, J., Sangan, C., Owen, J. M., and Lock, G. D., 2020, "Design and Testing of a Rig to Investigate Buoyancy-Induced Heat Transfer in Aero-Engine Compressor Rotors," ASME *J. Eng. Gas Turbines Power*.

[24] Pountney, O., Patinios, M., Tang, H., Luberti, D., Sangan, C., Scobie, J., Owen, J. M., and Lock, G. D., 2020, "Calibration of Thermopile Heat Flux Gauges Using a Physically-Based Equation," *Journal of Power and Energy*. [Accepted for publication]

[25] Tang, H., and Owen, J. M., 2020, "Effect of Radiation Inside Compressor Rotors," *ASME J. Turbomach*. [Accepted for publication]

[26] Owen, J. M., and Tang H., 2015, "Theoretical Model of Buoyancy-Induced Flow in Rotating Cavities," *ASME J. Turbomach.*, **137**(11), p. 111005.